

# Investigating the nature of the $z \simeq 2.8$ submillimeter selected galaxy SMM J02399–0136 with VLT spectropolarimetry\*

J. Vernet<sup>1,2</sup> and A. Cimatti<sup>2</sup>

<sup>1</sup> European Southern Observatory, Karl Schwarzschild Str. 2, 85748 Garching bei München, Germany

<sup>2</sup> Osservatorio Astrofisico di Arcetri, Largo E. Fermi, 50125 Firenze, Italy

Received 8 August 2001 / Accepted 18 September 2001

**Abstract.** We present deep optical spectropolarimetry of SMM J02399–0136 ( $z = 2.8$ ) done with the VLT *Antu* 8.2 m telescope equipped with FORS1. Moderate continuum and emission line polarization are measured ( $P \sim 5\%$ ). We do not detect broad lines in scattered flux as would be expected for a type-2 object but rather a polarization behaviour similar to BAL quasars. This classification is confirmed by the detection of both high and low ionization broad absorption troughs and a very red continuum. We argue that this object shares several properties with local ULIGs such as Mrk 231 and other ultraluminous infrared Lo-BAL quasars. However, the fact that the ultraviolet spectrum is dominated by non-stellar radiation does not prove that the dust that is thermally radiating in the far infrared is predominantly heated by the AGN. Since the energy that we get in the far-infrared is precisely that which is removed from the ultraviolet spectrum, this could mean that the starburst is more dust-enshrouded than the AGN due to a peculiar dust distribution. The limits we place on the putative starburst contribution to the restframe ultraviolet continuum together with constraints on the amount of extinction provide an upper limit to the star formation rate of about  $2000 M_{\odot} \text{ yr}^{-1}$ , consistent with previously claimed high star formation rates level in this object.

**Key words.** galaxies: active – galaxies: starburst – quasars: absorption lines – techniques: polarimetric – individual: SMM J02399–0136

## 1. Introduction

Recent submillimeter observations revealed a population of dusty ultraluminous infrared galaxies (ULIGs;  $L > 10^{12} L_{\odot}$ ) at high redshifts (e.g. Smail et al. 1997; Barger et al. 1998; Hughes et al. 1998; Cimatti et al. 1998). Understanding the nature of such galaxies is important in order to verify if they are the progenitors of the present-day massive spheroidals and whether massive galaxies formed through an episode of rapid and strong star formation. During such a starburst phase, a large amount of dust would be produced and the rest-frame ultraviolet (UV) radiation of OB stars would be absorbed by the dust grains and re-emitted in rest-frame far-infrared (FIR), thus making these galaxies strongly extincted at UV-optical wavelengths, but very luminous in the rest-frame FIR.

The inferred rest-frame FIR luminosities of the submm galaxies are very high ( $L > 10^{12-13} L_{\odot}$ ), thus implying star formation rates (SFRs) of the order of  $500\text{--}2000 M_{\odot} \text{ yr}^{-1}$ . The presence of large reservoirs of molecular gas available to form stars has been confirmed through the detection of CO emission in a few submillimeter selected galaxies ( $M_{\text{H}_2} \sim \times 10^{11} M_{\odot}$ ; Frayer et al. 1998b, 1999; Andreani et al. 2000).

However, such high SFRs are usually derived assuming that the dust is heated by young massive stars only and without any contribution from an active galactic nucleus (AGN) possibly present. In fact, if a quasar nucleus is hidden in the dust, its UV radiation could significantly contribute to the FIR luminosities, and the SFRs would be overestimated by large factors, thus leading to an incorrect estimate of the contribution of these galaxies to the global star formation history of the Universe (see Barger et al. 2000). We recall here that the same problem is present in low redshift ULIGs (see Sanders & Mirabel 1996 for a review).

In a first attempt to investigate the nature of high- $z$  submillimeter selected galaxies and the link between AGN

Send offprint requests to: J. Vernet,  
e-mail: vernet@arcetri.astro.it

\* Based on observations collected at the European Southern Observatory, Paranal, Chile (ESO Programme 64.P-0072).

and starburst activity in these sources, we observed SMM J02399–0136, a  $z = 2.8$  galaxy discovered as the counterpart of a SCUBA source found in a survey at  $850 \mu\text{m}$  of lensing cluster of galaxies (Ivison et al. 1998 [I98 hereafter]). Its inferred unlensed FIR luminosity is about  $10^{13} L_{\odot}$ , placing this object in the class of “hyperluminous” infrared galaxies, and the SFR estimated by I98 was in the range of  $2000\text{--}6000 M_{\odot} \text{yr}^{-1}$ . Thanks to the gravitational lensing of the cluster (whose amplification factor is known to be 2.5), the flux from this galaxy is high enough to provide a natural laboratory for detailed studies. For this reason, as a “pilot” study, we performed optical spectropolarimetry with the ESO Very Large Telescope (VLT) with the main aim of studying the AGN and starburst activities of this galaxy.

Throughout this paper we assume  $H_0 = 50 \text{ km s}^{-1} \text{ Mpc}^{-1}$ ,  $\Omega_0 = 1$  and  $\Omega_{\Lambda} = 0$  unless otherwise stated.

## 2. Observations and data reduction

Spectropolarimetric observations were carried out using the imaging spectrograph FORS1 (Appenzeller et al. 1992) in PMOS mode at the VLT 8.2 m unit telescope 1 (Antu) on December 1, 1999. The detector is a Tek.  $2048 \times 2048$  CCD with  $24 \mu\text{m}$  pixels which correspond to a scale of  $0.2'' \text{ pixel}^{-1}$ . The polarization optics of the instrument are composed of a Wollaston prism for beam separation and a rotating achromatic half-wave plate mosaic. A  $1''$  wide slit was used for all science observations. We used the 300 lines  $\text{mm}^{-1}$  grism (GRISM\_300V) providing a dispersion of  $\sim 2.6 \text{ \AA pixel}^{-1}$  and an effective resolution of about  $11 \text{ \AA FWHM}$ . Observations were divided into three sets of four exposures each of 1500 s with the half-wave plate position angles set to  $0^\circ$ ,  $22.5^\circ$ ,  $45^\circ$  and  $67.5^\circ$  to reach a total exposure time of 5 hours. The slit was oriented at  $88.6^\circ$  in order to include the two main components L1 and L2 of SMM J02399–0136 (see I98). All observations were done under subarcsecond seeing conditions with a seeing better than  $0.6''$  during the last polarimetric set.

After debiasing and flat-fielding, the spectra were cleaned for cosmic ray hits. The brightest component L1 is dominated by an unresolved source and was extracted using a  $1.8''$  aperture, whereas L2 is more extended and was extracted using a  $2''$  aperture. Wavelength calibration was done using HgCd, He and Ar arc spectra. After accurate wavelength registration using sky lines, the spectra were combined to form the Stokes parameters  $Q$  and  $U$  following the method described in Cohen et al. (1995). Unbiased values for the fractional polarization were estimated with the best estimator given by Simmons & Stewart (1985). Statistical confidence intervals on the fractional polarization and the polarization angle were determined using a Monte-Carlo simulation taking into account the effect background polarization and the detector noise (see Vernet 2001 for more details). We checked the polarimeter observing the null polarization standard

HD 64299. The measured polarization in the  $B$  band is  $P = 0.1295 \pm 0.0063\%$ , consistent with  $P = 0.151 \pm 0.032\%$  given by Turnshek et al. (1990). The polarization angle ( $\theta$ , position angle of the  $\mathbf{E}$ -vector) was corrected for effects of the half-wave plate fast axis rotation with wavelength using calibration data obtained during the instrument commissioning provided by ESO. The position angle offset between the half-wave plate coordinate and the sky coordinates was checked against values obtained for the polarized standard HD 251204. Discrepant values for the polarization angle of this star are reported in the literature. We measure  $\theta = 153.67 \pm 0.055^\circ$  in the  $V$  band, within  $2^\circ$  from the value measured by Ogle et al. (1999) using the Keck polarimeter (LRISp). The flux calibration was done using observations of the spectrophotometric standard star LTT 3218 (Hamuy et al. 1992), and the atmospheric extinction correction was done using CTIO extinction data since no extinction measurements for the Paranal observatory are yet available. Finally, the total flux spectra were corrected for Galactic extinction using  $A_B = 0.135 \text{ mag}$  from Schlegel et al. (1998) maps and the extinction curve from Cardelli et al. (1988). Integrating the spectrum over the  $R$  band gives  $R \simeq 22.5$ , close to the published value of  $22.60 \pm 0.04$  given in Ivison et al. (1998).

## 3. Results

### 3.1. Polarization results

Spectropolarimetry results for the brightest component L1 are displayed in Fig. 1. Data were binned to follow the main spectral features and to avoid strong sky lines while keeping a reasonable signal to noise ratio. Moderate continuum polarization is detected in all continuum bins. Continuum polarization measurement with  $1\sigma$  confidence interval in a single large bin in the line free region between  $\text{HeII}\lambda 1640$  and  $\text{CIII}\lambda 1909$  ( $6320 \leq \lambda_{\text{obs}} \leq 6990 \text{ \AA}$ ) gives  $P = 4.0 \pm 0.4\%$  and  $\theta = 102.2 \pm 3.3$ . Similarly between  $\text{Nv}\lambda 1240$  and  $\text{SiIV}\lambda\lambda 1393, 1402$  ( $4760 \leq \lambda_{\text{obs}} \leq 5150$ ) we find  $P = 6.5 \pm 0.7\%$  and  $\theta = 97.5 \pm 3^\circ$ . While the continuum polarization increases slightly to the blue, the polarization angle is weakly dependent on wavelength. Note however that the two extreme wavelength bins in Fig. 1 seem to indicate a rotation of  $\theta$  of about  $10^\circ$ .

$\text{Ly}\alpha$  and  $\text{Nv}$  lines show a significantly lower but still significant polarization than the neighboring continuum. After correction for underlying continuum polarization we find  $P_{\text{Ly}\alpha} = 2.1_{-0.5}^{+0.9}\%$  and  $P_{\text{Nv}} = 2.6_{-0.6}^{+1.0}\%$ . Polarization does not vary significantly within measurement errors across the  $\text{SiIV}$ ,  $\text{CIV}\lambda\lambda 1548, 1550$ ,  $\text{HeII}$  and  $\text{CIII}$  lines (note however that  $\text{CIV}$  line polarization is uncertain because it is affected by the relatively strong  $5890 \text{ \AA}$  Na D atmospheric emission line).

We have measured the polarization in the two broad troughs blueward of  $\text{CIV}$ . We find  $P = 17_{-3}^{+4}\%$  and  $P = 13_{-2}^{+4}\%$  in the bluest and in the reddest trough respectively, significantly higher than the neighboring continuum.

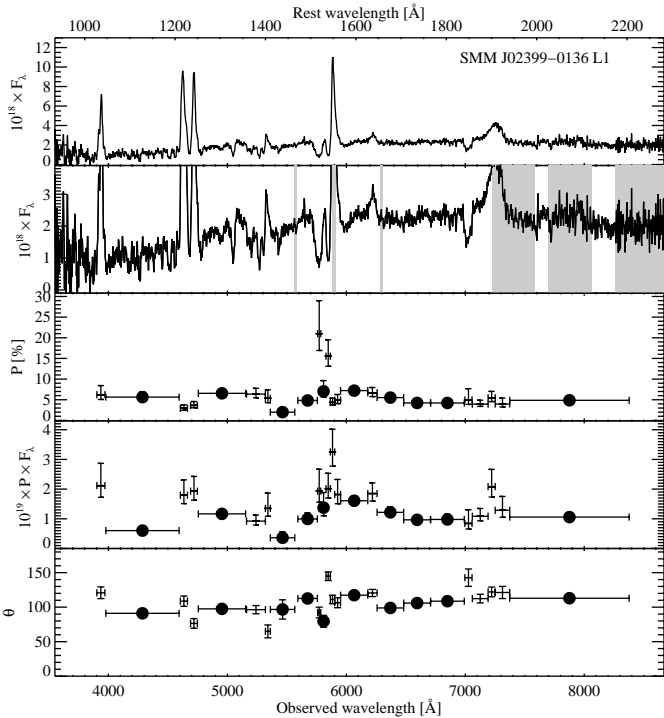


**Fig. 1.** Spectral and polarization properties of the main component L1. In each panel, *from top to bottom*: the observed total flux spectrum  $F_\lambda$  in units of  $10^{-18} \times \text{erg s}^{-1} \text{cm}^{-2} \text{\AA}^{-1}$  plotted on two different scales, the first to show strong emission lines and the second to show details of the continuum and absorption troughs, the percentage polarization with  $1\sigma$  error bars, the polarized flux in units of  $10^{-19} \times \text{erg s}^{-1} \text{cm}^{-2} \text{\AA}^{-1}$  and the position angle of the electric vector with  $1\sigma$  error bars. Filled circles and crosses respectively indicate continuum bins and emission lines bins with their underlying continuum. Shaded areas indicate regions of strong sky emission. The spectrum has been corrected for *A* and *B* band telluric absorptions.

As a result, the absorption features are absent in the polarized spectrum (see Fig. 1). We measure a C IV line *FWHM* in polarized flux of  $\sim 1930 \pm 730 \text{ km s}^{-1}$ , within the range of line width measurements for other strong lines in total flux. However, given the low signal to noise level within the small bins used to measure  $P$  in the troughs, such a result should be regarded with caution.

A consequence of the moderate polarization is the rather low signal to noise on the polarization measurements for such a faint target which forces us to apply a coarse binning to the data. This renders difficult the detection of shallow features such as broad emission lines in polarized flux. We find no evidence for the presence of broad emission line features in polarized flux in our data.

Polarization measurements for the component L2 are much more difficult and uncertain since it is about two magnitudes fainter than L1. We estimated the continuum polarization in a single large bin giving  $P = 9 \pm 3\%$  ( $3\sigma$  interval) and  $\theta = 140^\circ \pm 4^\circ$  ( $1\sigma$  error). This values should however be considered with caution because at such a low signal to noise level any residual of cosmic hits or imperfect

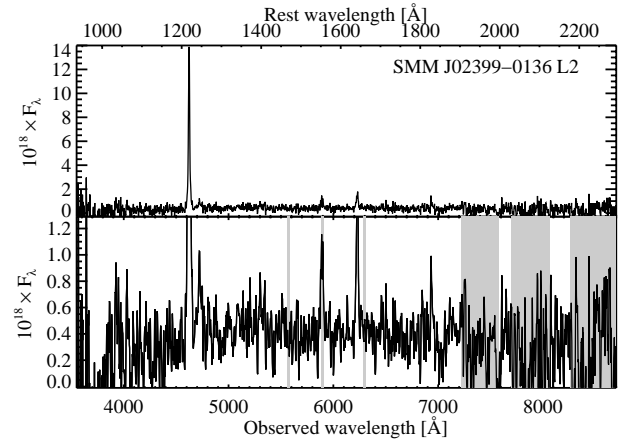


**Fig. 2.** Spectrum of the L2 component in units of  $10^{-18} \times \text{erg s}^{-1} \text{cm}^{-2} \text{\AA}^{-1}$  plotted on two different scales. The spectrum in the bottom panel has been smoothed using a 3 pixels boxcar.

bright sky line subtraction can have dramatic effects on polarization measurements.

### 3.2. Total flux spectrum

A consequence of the long integration time required by spectropolarimetric observations is the obtaining of a very deep total flux spectrum ( $S/N \sim 15$  per continuum resolution element for L1) allowing for the detection of several previously undetected absorption features in L1 and emission lines in L2. The total flux spectrum of L1 is presented on the top two panels in Fig. 1 and the spectrum of L2 in Fig. 2 on two different scales.

Component L1 shows a very red continuum with a slope  $\beta_{1500} = 0.6 \pm 0.2$  (with  $F_\lambda \propto \lambda^\beta$  measured between  $1300 < \lambda_{\text{rest}} < 1800 \text{\AA}$ ). The shape of the continuum is rather complex especially between Ly $\alpha$  and C IV probably due to blending of several absorption and emission features. The continuum of L2 is also well detected and is roughly flat in  $F_\lambda$  ( $\beta \sim 0$ ).

Emission line measurements and identifications for each component are given in Table 1. As reported in I98 and Villar-Martín et al. (1999) [VM99 hereafter], the Ly $\alpha$  line emission extends over  $13''$ , far beyond the extent of the detectable continuum (see Fig. 3). We do not detect extended emission in other strong emission lines. The observed emission line properties of L1 are consistent with the ones found in the spectra presented in I98 and VM99, except for the Ly $\alpha$  which is significantly stronger in VM99 probably because their L1 spectrum was extracted using a wider aperture. The strong emission lines have a typical width of  $\sim 2000 \text{ km s}^{-1}$ . Si IV and C IV show strongly asymmetric profiles due to absorption troughs of their blue wing. Ly $\alpha$ , C IV and N V line profiles do not show evidence of broad wings. C III] is remarkably broad compared to other lines, probably due to blending with Fe III UV 34  $\lambda\lambda 1895, 1914, 1926$  and Si III]  $\lambda\lambda 1882, 1892$  (see discussion).

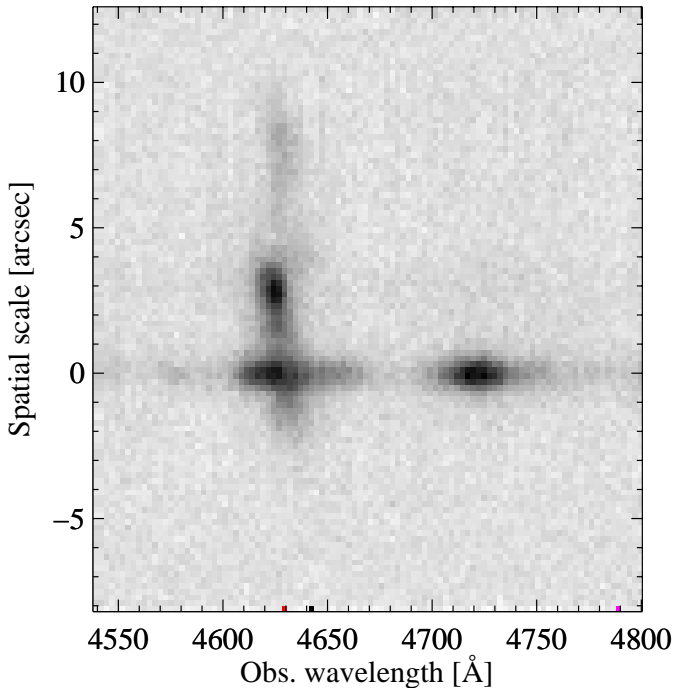


**Fig. 3.** The 2D-spectrum of SMM J02399–0136 in the region of the Ly $\alpha$  and NV emission lines. The origin of the spatial scale is set at the continuum peak of L1. The Ly $\alpha$  emission of the L2 component is clearly visible about 3'' away from L1, but the continuum is very weak. The total extent of the Ly $\alpha$  halo is about 13''.

Strong emission lines are also well detected in L2. The line ratios are very different from the ones observed in L1, in particular Ly $\alpha$ /CIV and HeII/CIV are much larger (see Table 1). The typical line width is of the order of 1000 km s<sup>-1</sup>, narrower than in L1. The Ly $\alpha$  line shows a broad (2200 km s<sup>-1</sup>) and a narrow (750 km s<sup>-1</sup>) component. We show in Fig. 4 a two component fit of this line. Note that the width of the broad component is similar to line widths measured in L1 (see Table 1).

We computed the redshift based on measurements of the HeII $\lambda$ 1640 line rather than other stronger emission lines because this recombination line is not affected by absorption. We find  $z = 2.7947 \pm 0.0004$  for L1, consistent with the redshift measured from the [O III] $\lambda\lambda$ 4959, 5007 in near infrared spectra by I98. Measurements for L2 give  $z = 2.7981 \pm 0.0003$  placing this second component about 270 km s<sup>-1</sup> from L1, also consistent with results found by I98 based on rest-frame optical lines.

One striking property of the spectrum of L1 is the presence of broad absorption lines (BAL). The presence of high ionization SiIV and CIV BAL was already noted by I98. We report here the new detection of low ionization absorption lines of AlIII $\lambda\lambda$ 1854, 1862, CII $\lambda\lambda$ 1334, 1336, SiII $\lambda\lambda$ 1304, 1309 and SiII $\lambda\lambda$ 1260, 1265. Observed wavelength and equivalent widths of the low ionization absorption lines are given in Table 2. Velocity profiles of the strongest absorption troughs are shown in Fig. 5. While high ionization lines have two main velocity complexes at

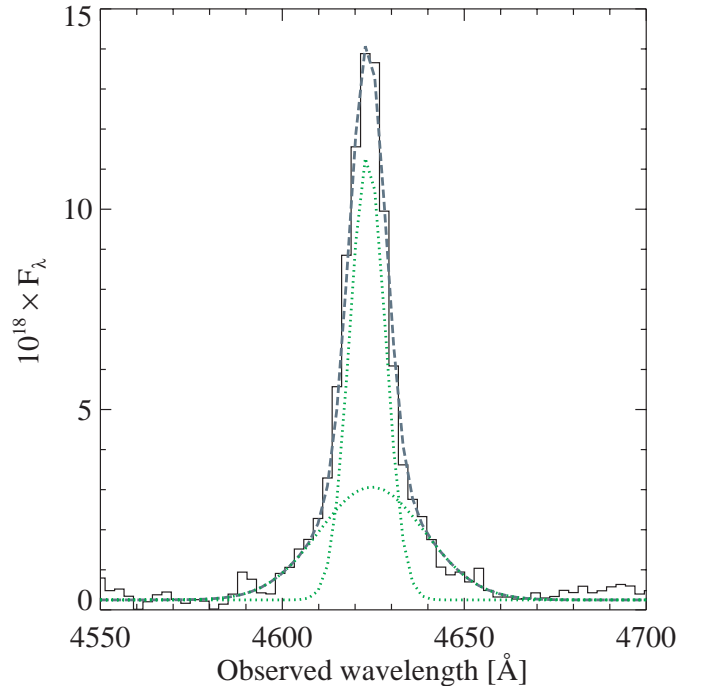


**Fig. 4.** Two components fit to the Ly $\alpha$  emission line profile in L2. Individual components are shown with dotted lines. The dashed line represents the total fit and the observed spectrum is displayed as a histogram. Parameters of the fit are given in Table 1.

–1000 and –6700 km s<sup>-1</sup>, low ionization absorption lines are only detected in the lowest velocity subcomponent.

## 4. Discussion

### 4.1. The origin of the polarization

Since this object suffers from very little Galactic extinction ( $E_{B-V} = 0.031$ , using the Schlegel et al. (1998) map and assuming  $R_V = 3.1$ ), we are confident that the observed polarization is intrinsic to SMM J02399–0136 (we find a limit to the interstellar polarization  $P \lesssim 0.28\%$  using the Serkowski (1975) formula  $P \leq 9 \times E_{B-V}\%$ ). Thus, the two mechanisms that can produce the observed level of both continuum and emission line polarization in the rest-frame ultraviolet are transmission of the radiation through magnetically aligned dust grains (dichroic polarization) within SMM J02399–0136 and scattering by electrons and/or by dust.

The possibility of dichroic polarization can be excluded considering the shape of  $P(\lambda)$ . The variation of  $P(\lambda)$  at ultraviolet wavelengths for polarization by transmission is well parameterized by an extended Serkowski law (Martin et al. 1999) obtained by fitting observations of different lines of sight in our Galaxy. It has a characteristic shape with a rather steep increase to the red and a maximum between 4000 and 7000 Å. Unless the polarization of SMM J02399–0136 is diluted by an extremely red unpolarized continuum component or its dust properties are very different from the Galactic ones, the increase of  $P(\lambda)$

**Table 1.** Emission line measurements.

Comp.	Id.	$\lambda_{\text{vac}}$ (Å)	$\lambda_{\text{obs}}$ (Å)	$F_{\lambda} \times 10^{17}$ (erg s <sup>-1</sup> cm <sup>-2</sup> )	$W_{\lambda}^{\text{obs}}$ (Å)	$FWHM$ (km s <sup>-1</sup> )	Comments
L1	O VI	1031.9, 1037.6	$3938.2 \pm 0.2$	$20.8 \pm 1.2$	$240 \pm 53$	2367	
	Ly $\alpha$	1215.7	$4628.9 \pm 0.1$	$34.4 \pm 0.3$	$235 \pm 7$	2383	2 components
	N V	1238.8, 1242.8	$4720.0 \pm 0.1$	$28.2 \pm 0.4$	$205 \pm 9$	1861	2 components
	Si IV	1393.8, 1402.8	$5334.6 \pm 0.1$	$3.7 \pm 0.2$	$21 \pm 1$	1899	blue wing absorbed
	C IV	1548.2, 1550.8	$5891.8 \pm 0.1$	$27.4 \pm 0.6$	$124 \pm 7$	1491	blue wing absorbed
	He II	1640.4	$6223.3 \pm 0.6$	$4.3 \pm 0.4$	$17.2 \pm 1.7$	2330	
	C III]	1906.7, 1908.7	$7247.9 \pm 0.5$	$27.5 \pm 0.7$	$122 \pm 8$	4672	probably blended with FeIII UV 34 and SiIII] lines (see text)
L2	Ly $\alpha$ narrow	1215.7	$4623.4 \pm 0.02$	$13.6 \pm 1.3$	$546 \pm 22$	744.2	
	Ly $\alpha$ broad	1215.7	$4624.6 \pm 0.7$	$10.2 \pm 1.4$	$419 \pm 103$	2212	
	N V	1238.8, 1242.8	$4723.3 \pm 0.8$	$1.64 \pm 0.5$	$40 \pm 17$	2026	broad and narrow comp.?
	C IV	1548.2, 1550.8	$5891.5 \pm 0.1$	$1.87 \pm 0.1$	$45.3 \pm 5.6$	1385	strong sky emission
	He II	1640.4	$6228.9 \pm 0.5$	$2.48 \pm 0.2$	$59.0 \pm 8.4$	963	

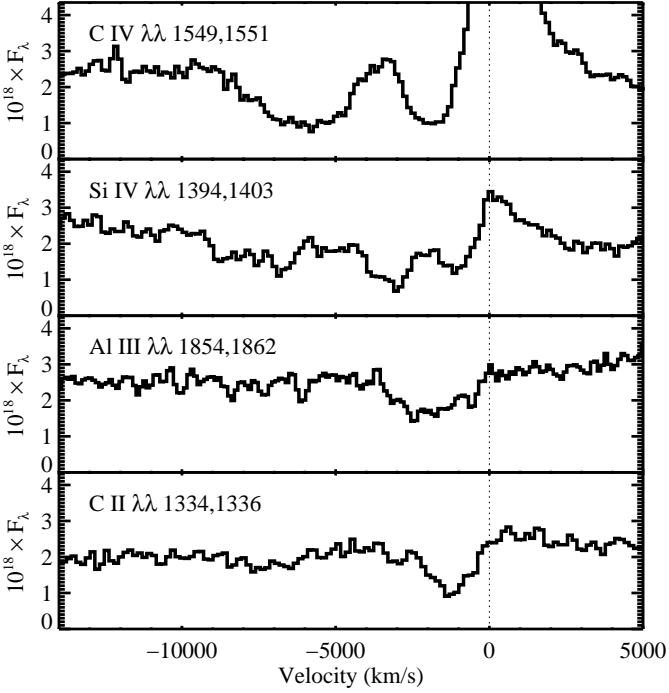


**Fig. 5.** Velocity profiles of the C IV  $\lambda\lambda$ 1549, 1550, Si IV  $\lambda\lambda$ 1394, 1403, Al III  $\lambda\lambda$ 1854, 1862, C II  $\lambda\lambda$ 1334, 1336 absorption troughs. The zero velocity is taken at the expected emission wavelength of the reddest component of the doublet, computed using the redshift determined with the He II line.

to the blue in L1 is not compatible with polarization by transmission. Therefore, we consider scattering by dust and/or electrons as the most likely dominant polarization mechanism.

**Table 2.** Low ionization absorption line measurements in L1.

Identification	$\lambda_{\text{vac}}$ (Å)	$\lambda_{\text{obs}}$ (Å)	$W_{\lambda}^{\text{obs}}$ (Å)
Si II	1260.4, 1264.7	4780	9
O I	1302.2, 1304.9	4948	8
Si II	1304.4, 1309.3		
C II	1334.5, 1335.7	5048	17
Al III	1854.7, 1862.8	7021	23

#### 4.2. The nature of the AGN

The two classes of objects that commonly show a significant amount of scattered light in their UV spectrum are type-2 AGN (i.e. Seyfert 2 and radio galaxies, see e.g. Antonucci & Miller 1985; di Serego Alighieri et al. 1989) and broad absorption line quasars (see e.g. Goodrich & Miller 1995). In type-2 objects, scattering is produced by material distributed on the kpc scale illuminated by the anisotropic radiation from an active nucleus surrounded by an optically thick torus that completely blocks the direct view to the quasar (see e.g. review by Antonucci 1993). The continuum of these objects is usually well resolved in the rest-frame UV and they typically show high continuum polarization and broad lines detected in scattered flux (up to 20%, see e.g. the spectropolarimetric study of  $z \sim 2.5$  radio galaxies by Vernet et al. 2001). In contrast, scattering is believed to occur much closer to the nucleus in BAL QSOs, while the unpolarized direct quasar radiation is less attenuated, resulting in a much smaller range in observed polarization (see e.g. spectropolarimetric study of a sample of BALQSO by Ogle et al. 1999 [O99 hereafter]).

The detection of moderate continuum polarization together with the non-detection of broad emission lines in scattered flux and the presence of broad absorption

troughs suggests that L1 is more similar to a BAL QSO than to a type-2 object. This interpretation is strengthened by the fact that L1 is dominated by a point source (the continuum emission is unresolved in our spectrum, even in data obtained with seeing  $\sim 0.5''$ ; I98 measure a  $FWHM$  of 0.1–0.2'' for L1 on HST WF/PC F702W and WFPC2 F336W images). The presence of low ionization absorption further identifies L1 as one of the very few low ionization BAL QSOs known (Lo-BAL QSO). While about 12% of known quasars show high ionization BAL (Weymann et al. 1991), a small subset of these (about 15%, Hutsemékers et al. 1998) also show low ionization broad absorption lines like  $MgII\lambda\lambda 2796, 2804$  and in some cases  $AlIII\lambda\lambda 1854, 1862$ .

The slow increase of the continuum polarization to the blue that we detect in L1 is very similar to what is commonly observed in BAL QSO (see O99). The polarization level of L1 is clearly sitting in the high tail of the polarization distribution of BAL QSO. This may however be not too surprising considering that Lo-BAL QSOs seem to show a wider range in polarization than high ionization BAL QSOs as suggested by Hutsemékers et al. (1998). Note that the strong rise in polarization that we possibly detect in the CIV absorption troughs is also a typical feature of BAL QSOs (e.g. O99). The very red color of the continuum ( $\beta_{1500} \simeq 0.6$ ) compared to normal quasars ( $\beta_{1500} \simeq -1.4$ , measured on Brotherton et al. 2001 composite quasar) is also a common feature observed in Lo-BAL QSO. Measuring the UV continuum slope on Brotherton et al. (2001) Lo-BAL QSO composite spectrum we find  $\beta_{1500} \simeq 0.4$ , rather close to the color of L1.

The width of the lines of L1 ( $\sim 2000 \text{ km s}^{-1} FWHM$ ) appears to be intermediate between that of quasars (typically  $\sim 5000 \text{ km s}^{-1}$ ) and type-2 objects ( $\sim 1000 \text{ km s}^{-1}$ ) while the line ratios are more typical of a quasar. Emission line modeling performed by VM99 suggests that the emission line spectrum of L1 might be dominated by an intermediate density region ( $n_H \simeq 10^4 - 10^6$ ). The only line that appears to have a broad and rather complex profile is  $CIII]\lambda 1909$ . Such a phenomenon has already been observed both in BAL QSO (Hartig & Baldwin 1986; Weymann et al. 1991) and narrow line quasars (e.g. Baldwin et al. 1988). In these objects, the apparent broad feature has usually been interpreted as a blend of  $CIII]\lambda 1909$ ,  $FeIII UV 34 \lambda\lambda 1895, 1914, 1926$  multiplet and  $SiIII]\lambda\lambda 1882, 1892$  doublet.

Properties of L2 are significantly different from those of L1. Line widths and line ratios are more typical of type-2 objects. This together with the detection of a broader Ly $\alpha$  component of a width similar to that of L1 and possible high continuum polarization suggests that the spectrum of L2 could be dominated by scattered light from the AGN present in L1, similar to the extended UV emission observed in high redshift radio galaxies.

SMM J02399–0136 shows quite different properties from the three high redshift hyperluminous infrared galaxies F 10214 + 4724, P 091004 + 4109 and F 15307 + 3252 that have been proven to be type-2 objects

(Goodrich et al. 1996; Tran et al. 2000; Hines et al. 1995). In fact, SMM J02399–0136 shares several of its unusual properties with the low redshift ULIG Mrk 231 that has also been classified as a Lo-BAL QSO (e.g. Smith et al. 1995). The nature of Lo-BAL QSO and in particular their link with ULIGs is not clear at present. It has been suggested that some of these objects could be AGN/massive starburst composite (Lipari et al. 1994) or young quasars casting off their cocoons of gas and dust (Sanders et al. 1988; Voit et al. 1993).

### 4.3. Constraints on the star formation activity

The strong CO(3 $\rightarrow$ 2) emission and the inferred large mass of molecular gas together with the high far-infrared luminosity indicate that star formation is occurring at a rate greater than  $\sim 10^3 M_{\odot} \text{ yr}^{-1}$  (I98; Frayer et al. 1998a). Although dilution of the polarization by starlight is not required by our spectropolarimetric data, a significant contribution of a population of hot stars to the UV continuum is not at all ruled out.

#### 4.3.1. Searching for starburst spectral signatures

The two unambiguous direct spectral signatures of the presence of young massive stars that we might expect to detect in the rest-frame UV are  $SiIV\lambda 1400$ ,  $CIV\lambda 1549$  P-Cygni profiles and purely photospheric absorption lines (i.e. not contaminated by interstellar absorption) from O and B stars such as  $SiIII\lambda 1294$ ,  $CIII\lambda 1427$ ,  $Sv\lambda 1502$  and  $NIV\lambda 1718$ .

Both the shape and the velocity extent of the troughs blueward of CIV and SiIV emission lines are not compatible with these features being dominated by stellar P-Cygni profiles. While we observe double absorption troughs that extend up to about  $-9000 \text{ km s}^{-1}$  with rather sharp edges both in CIV and SiIV lines (see Fig. 5) in L1, stellar wind absorption troughs are in general strongly asymmetric and extend no further than about  $-5000 \text{ km s}^{-1}$  in both modeled starburst spectra (e.g. Starburst 99) and observed star-forming galaxies (see e.g. local starburst galaxies templates NGC 1705, NGC 1741, NGC 4214 and IRAS 0833+6517 from Heckman & Leitherer 1997; Conti et al. 1996; Leitherer et al. 1996; Gonzalez Delgado et al. 1998 respectively and also the  $z = 2.7$  lensed Lyman break galaxy MS 1512–cB58 from Pettini et al. 2000).

We detect one absorption line at  $\lambda_{obs} = 5434.4 \text{ \AA}$  ( $\lambda_{rest} = 1432.1 \text{ \AA}$ ) relatively close to the expected wavelength of the  $CIII\lambda 1427$  photospheric line. However, its equivalent width ( $W_{\lambda}^{rest} = 1.75 \pm 0.1 \text{ \AA}$  in the rest-frame) is significantly larger than the maximum equivalent width of  $\sim 1 \text{ \AA}$  that we measured for this line on both the above listed starburst templates and Starburst 99 models. One more likely identification for this feature is that of a  $MgII\lambda\lambda 2796, 2803$  doublet due to an intervening absorber. A two Gaussian fitting of this absorption feature yield  $\lambda_{obs} = 5431.7 \text{ \AA}$  and

$\lambda_{\text{obs}} = 5445.8 \text{ \AA}$  with an error of  $\sim 0.5 \text{ \AA}$ , consistent with a MgII $\lambda$ 2796, 2803 doublet at  $z = 0.9424 \pm 0.0002$ .

#### 4.3.2. Limits on the stellar continuum

Since we did not find any direct spectral evidence for the presence of a massive starburst in our spectrum, we used two different methods to constrain the fraction of stellar continuum to the total flux ( $f^*$ ).

**First method.** We first computed an upper limit to the equivalent width of an unresolved line at the expected wavelength of the four purely photospheric lines listed above. We found the most stringent limit for the NIV $\lambda$ 1718 line: in the region of the expected observed wavelength ( $\sim 6521 \text{ \AA}$ ), the continuum signal to noise ratio is  $\sim 16$  which gives a  $2\sigma$  upper limit on the rest-frame equivalent width of the NIV $\lambda$ 1718 line of  $\sim 0.4 \text{ \AA}$ . The equivalent width of this photospheric absorption line measured on both continuous star formation and instantaneous burst Starburst 99 model spectra (Salpeter IMF, solar metallicity) ranges from  $0.6$  to  $0.7 \text{ \AA}$  for bursts ages  $t^*$  between  $1$  and  $5 \text{ Myr}$ . This value is comparable to what is typically measured in local starbursts (e.g. in Heckman & Leitherer 1997 HST/GHRS spectrum of NGC 1705 we measure  $W_\lambda(\text{NIV}) \sim 0.6$ ). These numbers together with our upper limit on the observed equivalent width allow us to put an upper limit to the contribution at  $1718 \text{ \AA}$  of a young ( $t^* \leq 5 \text{ Myr}$ ) starburst of about  $70\%$  of the total flux ( $f^*(1718) \lesssim 70\%$ ).

**Second method.** Since we showed that the observed absorption troughs are intrinsic to the active nucleus, we can also place an upper limit to  $f^*$  by saying that the stellar continuum level has to be lower than the flux at the center of the absorption troughs (that is to say that if these BAL troughs were saturated then the stellar flux would be precisely equal to the flux at the bottom of the troughs). Considering the deepest CIV trough we obtain that the stellar continuum flux  $F_\lambda^*(1500)$  at  $\sim 1500 \text{ \AA}$  must be lower than  $9.5 \times 10^{-19} \text{ erg s}^{-1} \text{ cm}^{-2} \text{ \AA}^{-1}$ . At  $\lambda_{\text{rest}} = 1500 \text{ \AA}$ , the measured total flux is  $\sim 2.3 \times 10^{-18} \text{ erg s}^{-1} \text{ cm}^{-2} \text{ \AA}^{-1}$ . This then gives a more stringent limit than the previous method:  $f^*(1500) \lesssim 40\%$ .

**Polarization level consistency check.** The lack of knowledge about the intrinsic AGN continuum polarization level prevents us from putting meaningful constraints on  $f^*$  using polarization measurements. We can however reversely compute, as a check, the limit on the intrinsic AGN polarization  $P_{\text{AGN}}$  given  $f^*$ : calling  $P_{\text{obs}}$  the observed polarization,  $P_{\text{AGN}}$  is given by  $P_{\text{AGN}} = P_{\text{obs}}/(1 - f^*)$ . For  $f^*(1500) \lesssim 40\%$ , taking  $P_{\text{obs}} \sim 5\%$  we find  $P_{\text{AGN}} \lesssim 8\%$ . This value is higher than the average BAL QSO continuum polarization but is comparable to what is observed in most polarized objects in O99's sample

(e.g.  $P = 5.41\%$  between  $1600 \text{ \AA}$  and  $1840 \text{ \AA}$  in the BAL QSO 1333+2840). Note also that this continuum polarization level is still moderate compared to that of the most polarized Lo-BAL quasar known FIRST J15633.8+351758 for which  $P \simeq 13\%$  near  $2000 \text{ \AA}$  (Brotherton et al. 1997).

#### 4.3.3. Limits on the star formation rate

We can now translate the most stringent limit we obtained on  $F_\lambda^*(1500)$  in the observed frame into a limit on the *SFR*. The luminosity distance at  $z = 2.794$  for the cosmology we assume in this paper is  $D_L = 6.83 \times 10^{28} \text{ cm}$ . The limit on the rest-frame stellar luminosity at  $1500 \text{ \AA}$  is then  $L_\nu^{\text{rest}}(1500) \lesssim 1.6 \times 10^{29} \text{ erg s}^{-1} \text{ Hz}^{-1}$ . Taking the Madau et al. (1998) conversion factor between *SFR* and luminosity at  $1500 \text{ \AA}$  ( $L_\nu(1500) = 8 \times 10^{27} \times \text{SFR}/[M_\odot \text{ yr}^{-1}]$ ) we obtain an upper limit to the *SFR* of  $\sim 20 M_\odot \text{ yr}^{-1}$ . If we take into account the lensing factor of  $2.5$  given by 198 we have  $\text{SFR} \lesssim 8 M_\odot \text{ yr}^{-1}$ .

We know that star formation is strongly affected by dust extinction, and we need to correct for this effect in order to set meaningful limits on the *SFR*. Any unpolarized stellar component that would contribute significantly to the continuum ( $f^* \geq 10\%$ ) would affect the observed dependence of the polarization on wavelength if its color is different from that of the AGN. In L1, we know that  $P(\lambda)$  rises weakly to the blue. Since this behavior is very similar to what is observed in most of the BAL QSO (see O99), we can assume that the amount of dilution by starlight does not vary significantly over the observed wavelength range which means that the stellar component must have a spectral slope similar to that of the total flux ( $\beta_{1500} \sim 0.6$ ). This slope is much redder than the one predicted by stellar population synthesis models for young (a few  $10^7 \text{ yr}$ ) populations indicating that star formation is heavily dust enshrouded, as suggested by the huge FIR luminosity of this object. Starburst 99 stellar population synthesis models predict a slope  $\beta_{1500}$  of about  $-2.5$  for a  $t^* \geq 10 \text{ Myr}$  continuous burst (i.e. when the stellar population has reached an equilibrium after the initial onset of the burst) which gives a continuum slope index variation due to reddening  $\Delta\beta_{1500} \sim 3.1$ . Assuming a Calzetti (1997) extinction law we compute the slope index variation  $\Delta\beta = -5.9 \times E_{B-V}$  and the extinction in magnitude at  $1500 \text{ \AA}$   $A_{1500} = 11.4 \times E_{B-V}$  as a function of reddening. This then gives  $E_{B-V} \sim 0.52$  and  $A_{1500} \sim 6.0 \text{ mag}$ , an extinction of a factor  $\sim 250$  at  $1500 \text{ \AA}$ .

Combining this estimate with our limit on the *SFR* we obtain an extinction corrected upper limit on the *SFR* of  $\sim 2000 M_\odot \text{ yr}^{-1}$ . How sensitive is this limit to our assumptions? Unless the observed absorption troughs do not originate from within the AGN, the limit on the stellar flux at  $1500 \text{ \AA}$  is quite reliable. This is in fact a rather conservative upper limit. However, our estimate of the extinction, based on considerations on polarization dilution by starlight, is valid only if the stellar continuum makes up a significant fraction of the total UV continuum.

If for instance  $f^*$  is lower than  $\sim 10\%$  at  $1500 \text{ \AA}$ , the limit on the  $SFR$  before extinction correction becomes as low as  $2 M_{\odot} \text{ yr}^{-1}$ . In this case we cannot constrain the extinction with the present data. It would then require an extinction factor of  $\sim 1000$  ( $A_{1500} \sim 7.5 \text{ mag.}$ ) to reach the above limit of  $2000 M_{\odot} \text{ yr}^{-1}$  or a factor  $\sim 3000$  ( $A_{1500} \sim 8.7 \text{ mag.}$ ) to reach the total  $SFR$  of  $\sim 6000 M_{\odot} \text{ yr}^{-1}$  derived by I98 from submillimeter data.

## 5. Conclusions

We have presented in this paper deep low resolution optical spectropolarimetry of the  $z \simeq 2.8$  submillimeter selected galaxy SMM J02399–0136. The main new observational results are the following:

- The main component L1 shows moderate ( $\sim 5\%$ ) continuum polarization. We also detect formally significant polarization of the second component L2. We do not find any evidence for the presence of broad scattered lines.
- We do not detect any unambiguous signature of massive stars like P-Cygni profiles or photospheric absorption lines in the rest-frame UV spectrum of this object.
- In addition to the already known high ionization absorption troughs, we discovered broad low ionization absorption lines (AlIII, CII and SiII).

While SMM J02399–0136 appears to be significantly different from other high- $z$  hyperluminous infrared objects that have been proven to be type-2 objects (F 10214 + 4724, P 091004 + 4109 and F 15307 + 3252), it shares several properties (continuum polarization, low ionization broad absorption lines) with the well-known nearby ULIG Mrk 231 and other polarized low ionization BAL quasars.

The fact that the spectrum is AGN dominated and that we do not see any direct sign of star formation activity in the ultraviolet spectrum does not necessarily mean that the dust that is thermally radiating in the FIR is predominantly heated by AGN. Since the energy that we get in the FIR is precisely that which is removed from the ultraviolet spectrum, this could just mean that the starburst is more dust enshrouded than the AGN due to a peculiar dust distribution. Indeed, our data allow for star formation rates as high as  $2000 M_{\odot} \text{ yr}^{-1}$ . This level of star formation is compatible with the large amount of molecular gas inferred from CO observations and with the huge FIR luminosity of this object.

Deep spectropolarimetric observations are powerful tools to disentangle AGN and starburst activity. They may help to find hidden AGN activity in putative “pure starbursts” galaxies. They can also help to constrain star formation rates and starburst properties “cleaned” from AGN activity, independently of submillimeter observations. Future detailed studies of the physical properties of more submillimeter selected objects may provide important clues to understand the link between AGN and starburst activity.

*Acknowledgements.* We thank Chris Lindman and Thomas Szeifert for their assistance during the observing run at Paranal Observatory. We also thank Robert Fosbury, Sperello di Serego Alighieri and Jacqueline Bergeron for interesting discussions and suggestions.

## References

- Andreani, P., Cimatti, A., Loinard, L., & Röttgering, H. 2000, *A&A*, 354, L1
- Antonucci, R. R. J., & Miller, J. S. 1985, *ApJ*, 297, 621
- Appenzeller, I., Duensing, K. H., Fricke, K., et al. 1992, in *Progress in Telescope and Instrumentation Technologies*, 577
- Baldwin, J. A., McMahon, R., Hazard, C., & Williams, R. E. 1988, *ApJ*, 327, 103
- Barger, A. J., Cowie, L. L., & Richards, E. A. 2000, *AJ*, 119, 2092
- Barger, A. J., Cowie, L. L., Sanders, D. B., et al. 1998, *Nature*, 394, 248
- Brotherton, M. S., Tran, H. D., Becker, R. H., et al. 2001, *ApJ*, 546, 775
- Brotherton, M. S., Tran, H. D., van Breugel, W., Dey, A., & Antonucci, R. 1997, *ApJ*, 487, L113
- Calzetti, D. 1997, in *The Ultraviolet Universe at Low and High Redshift: Probing the Progress of Galaxy Evolution*, 403
- Cardeli, J. A., Clayton, G. C., & Mathis, J. S. 1988, *ApJ*, 329, L33
- Cimatti, A., Andreani, P., Röttgering, H., & Tilanus, R. 1998, *Nature*, 392, 895
- Cohen, M. H., Ogle, P. M., Tran, H. D., et al. 1995, *ApJ*, 448, L77
- Conti, P. S., Leitherer, C., & Vacca, W. D. 1996, *ApJ*, 461, L87
- di Serego Alighieri, S., Fosbury, R. A. E., Tadhunter, C. N., & Quinn, P. J. 1989, *Nature*, 341, 307
- Frayser, D. T., Ivison, R. J., Scoville, N. Z., et al. 1999, *ApJ*, 514, L13
- Frayser, D. T., Ivison, R. J., Scoville, N. Z., et al. 1998a, *ApJ*, 506, L7
- Frayser, D. T., Seaquist, E. R., & Frail, D. A. 1998b, *AJ*, 115, 559
- Gonzalez-Delgado, R. M., Leitherer, C., Heckman, T., et al. 1998, *ApJ*, 495, 698
- Goodrich, R. W., & Miller, J. S. 1995, *ApJ*, 448, L73
- Goodrich, R. W., Miller, J. S., Martel, A., et al. 1996, *ApJ*, 456, L9
- Hamuy, M., Walker, A. R., Suntzeff, N. B., et al. 1992, *PASP*, 104, 533
- Hartig, G. F., & Baldwin, J. A. 1986, *ApJ*, 302, 64
- Heckman, T. M., & Leitherer, C. 1997, *AJ*, 114, 69
- Hines, D. C., & Wills, B. J. 1995, *ApJ*, 448, L69
- Hughes, D. H., Serjeant, S., Dunlop, J., et al. 1998, *Nature*, 394, 241
- Hutsemekers, D., Lamy, H., & Remy, M. 1998, *A&A*, 340, 371
- Ivison, R. J., Smail, I., Le Borgne, J. F., et al. 1998, *MNRAS*, 298, 583
- Leitherer, C., Vacca, W. D., Conti, P. S., et al. 1996, *ApJ*, 465, 717
- Lipari, S. 1994, *ApJ*, 436, 102
- Madau, P., Pozzetti, L., & Dickinson, M. 1998, *ApJ*, 498, 106
- Martin, P. G., Clayton, G. C., & Wolff, M. J. 1999, *ApJ*, 510, 905

- Ogle, P. M., Cohen, M. H., Miller, J. S., et al. 1999, *ApJS*, 125, 1
- Sanders, D. B., & Mirabel, I. F. 1996, *ARA&A*, 34, 749
- Sanders, D. B., Soifer, B. T., Elias, J. H., et al. 1988, *ApJ*, 325, 74
- Schlegel, D. J., Finkbeiner, D. P., & Davis, M. 1998, *ApJ*, 500, 525
- Serkowski, K., Mathewson, D. L., & Ford, V. L. 1975, *ApJ*, 196, 261
- Simmons, J. F. L., & Stewart, B. G. 1985, *A&A*, 142, 100
- Smail, I., Ivison, R. J., & Blain, A. W. 1997, *ApJ*, 490, L5
- Smith, P. S., Schmidt, G. D., Allen, R. G., & Angel, J. R. P. 1995, *ApJ*, 444, 146
- Tran, H. D., Cohen, M. H., & Villar-Martin, M. 2000, *AJ*, 120, 562
- Turnshek, D. A., Bohlin, R. C., Williamson, R. L., Lupie, O. L., & Koornneef, J. 1990, *AJ*, 99, 1243
- Vernet, J. 2001, Ph.D. Thesis, Université Paris VII
- Vernet, J., Fosbury, R. A. E., Villar-Martín, M., et al. 2001, *A&A*, 366, 7
- Villar-Martín, M., Fosbury, R. A. E., Binette, L., Tadhunter, C. N., & Rocca-Volmerange, B. 1999, *A&A*, 351, 47
- Voit, G. M., Weymann, R. J., & Korista, K. T. 1993, *ApJ*, 413, 95
- Weymann, R. J., Morris, S. L., Foltz, C. B., & Hewett, P. C. 1991, *ApJ*, 373, 23